Is That Really Your Strehl Ratio?

Lewis C. Roberts Jr.[a], Marshall D. Perrin[b], Franck Marchis[b], Anand Sivaramakrishnan[c], Russell B. Makidon[c], Julian C. Christou[d], Bruce A. Macintosh[e], Lisa A. Poyneer[e], Marcos A. van Dam[e] and Mitchell Troy[f]

[a]The Boeing Company, 535 Lipoa Pkwy, Suite 200, Kihei HI 96753

[b]University of California, Berkeley, Department of Astronomy, 601 Campbell Hall Berkeley CA 94720

[c]Space Telescope Science Institute, 3700 San Martin Drive, Baltimore MD 21218

[d]Center for Adaptive Optics, University of California, Santa Cruz, 1156 High St, Santa Cruz, CA 95064

[e]Lawrence Livermore National Laboratory, IGPP, 7000 East Ave., L-413, Livermore CA 94551

[f]Jet Propulsion Laboratory, California Institute of Technology, 4800 Oak Grove Drive, Pasadena CA 91109

ABSTRACT

Strehl ratio is the most commonly used metric for adaptive optics (AO) performance. It is also the most misused metric. Every Strehl ratio measurement algorithm has subtle differences that result in different measured values. This creates problems when comparing different measurements of the same AO system and even more problems when trying to compare results from different systems.

To determine how much the various algorithm difference actually impacted the measured values, we created a series of simulated point spread functions (PSF). The simulated PSFs were then sent around to the various members of the project who then measured the Strehl ratio. The measurements were done blindly, with no knowledge of the true Strehl ratio. We then compared the various measurements to the truth values. Each measurement cycle turned up impacts which were further investigated in the next cycle. We present the results of our comparisons showing the scatter in measured Strehl ratios and our best recommendations for computing an accurate Strehl ratio.

Keywords: Adaptive Optics, Strehl Ratio, Image quality

1. INTRODUCTION

A Strehl ratio is the ratio of the peak intensity of a measured point spread function (PSF) to the peak intensity of a perfect diffraction-limited PSF for the same optical system,

$$S = \frac{I(\mathbf{x} = 0)}{P(\mathbf{x} = 0)}, \tag{1}$$

where $\mathbf{x}$ is the position vector, $I(\mathbf{x} = 0)$ is the maximum of the measured point spread function (PSF) and $P(\mathbf{x} = 0)$ is the maximum of the diffraction limited PSF.[1]

In the astronomical world, the Strehl ratio is most commonly used in the analysis of adaptive optics (AO) performance, though it can be used to assess the image quality of any image. In AO it is used for several purposes. One common example is nightly imaging sharpening of an AO system. Here the Strehl ratio is measured repeatedly for the same source while parameters of the AO system are adjusted to maximize the Strehl ratio. In this usage, the absolute Strehl ratio does not matter so much as the relative changes in Strehl ratio between successive images.

Advancements in Adaptive Optics, edited by Domenico Bonaccini Calia, Brent L. Ellerbroek, Roberto Ragazzoni, Proceedings of SPIE Vol. 5490 (SPIE, Bellingham, WA, 2004)
0277-786X/04/$15 · doi: 10.1117/12.549115

A Strehl ratio can also be used as a measure of system performance. In this case, the measured Strehl ratio is compared to a design specification or what a simulation predicts. This gives a useful metric for determining if the AO system needs to be improved. Often the Strehl ratio is broken down into the Strehl ratio of each individual optical component in the AO system. The Strehl ratio is related to the wave-front errors via the Maréchal approximation,[2]

$$S = \exp[-\sigma_\phi^2] \exp[-\sigma_\chi^2], \tag{2}$$

where σ_ϕ^2 is the wave-front phase variance and σ_χ^2 is the variance of the log-normal amplitude at the pupil plane. The Maréchal approximation shows that the total Strehl ratio is the product of the Strehl ratios of the individual components as long as the phase errors of each component are uncorrelated. This allows the determination of which component needs to be improved to yield a overall system improvement. It can also be used to generate an estimate of the overall phase error in the system.

Strehl ratio is used to compare the performance of different AO systems. This can be used to compare efficacy of different designs or techniques or to determine which AO system to best suited for a given experiment. Strehl ratio can also be used in data analysis, to determine if a given image is good enough to supply the needed information.

There is no standard method for determining the Strehl ratio of a given PSF. Most of the research groups working in AO have independently developed software packages for measuring the Strehl ratio. As a result, Strehl ratios reported in the literature are computed using algorithms which differ in their details, rendering comparison of Strehl ratios from different instruments difficult. Another difficulty in comparing AO systems is that many groups do not publicize their average or typical Strehl ratios, but only a few select measured Strehl ratios.

To investigate the degree in which the biases in different algorithms result in divergent Strehl ratio measurements, we started a systematic campaign of measuring the Strehl ratios of simulated data. We generated simulated AO PSFs for which the true Strehl ratio was known, as we have perfect knowledge of the simulated wavefront. By applying Strehl ratio codes used with a variety of AO systems (including the twin 10 m Keck telescopes, the 3 m Shane telescope at Lick Observatory, the the Hale 5 m at Palomar, the AEOS 3.6 m and the 8 m Very Large Telescopes) to this synthetic dataset, we were able to quantify the degree of scatter between Strehl ratio algorithms, and to begin to identify best practices for Strehl ratio measurement.

2. SIMULATION METHODOLOGY

We used two different methods of creating artificial PSFs, performed independently by two individuals using simulation software with no common heritage. This allows us to hopefully eliminate any biases in the simulation methods. In both cases the simulations used the Palomar 5 meter Hale pupil geometry (Primary diameter of 4.88 m and a secondary obscuration of 1.8 m), and varied the simulated AO performance to generate a series of simulated H-band (1.65 μm) images covering a range of Strehl ratios.

2.1. Method One

In the first method, PSFs were constructed using a Fourier-domain Monte Carlo simulation code. A series of random realizations of a Kolmogorov atmosphere were generated. The DM response was generated by applying a Fourier filter to the data representing the AO system influence function. Wavefront measurement noise was then added in, as white noise filtered by the same influence function. The resulting shape was subtracted from the atmospheric phase. Typically 100 realizations of the atmosphere were used to generate each PSF. The telescope pupils used were a pixelated version of a circular telescope with a circular secondary obscuration and no secondary supports.

2.2. Method Two

The second method characterizes each simulation by the telescope entrance pupil size and geometry, the seeing, D/r_o, the number of actuators across the primary, N_{act} and the linear size of the array, N_s, sampling the incoming wavefront.

We generate a series of independent realizations of Kolmogorov-spectrum phase screens in $2N_s$ by $2N_s$ arrays, with the spatial sampling of these arrays chosen to provide several samples across each Fried length r_o. We Fourier transform the input phase arrays, and multiply them by a high-pass filter to mimic the action of AO. Then we reverse-transform the filtered arrays to obtain the AO-corrected wavefront.

We use a parabolic high-pass filter in spatial frequency space to simulate AO, as described in Sivaramakrishnan et al. (2001).[3] To avoid edge effects introduced by the Fourier filtering, only the central N_s by N_s section of the filtered array is retained. This is then multiplied by a binary mask representing the telescope entrance pupil. This mask is opaque (zero) outside the primary mirror edge, and inside the secondary obstruction. Secondary support spiders, mirror surface micro-roughness and scattering have not considered in these simulations.

We embed the filtered and masked array in the center of an $8N_s$ by $8N_s$ zero-filled array. This results in image field sampling of $\lambda/8D$, which allows for effective comparison and binning of simulated images down to $\lambda/4D$ and $\lambda/2D$ pixels.

We then create the complex phasor $e^{i\phi(x,y)}$ describing the electric field corresponding to the phase $\phi(x,y)$, and Fourier transform the phasor to obtain the image field.

For these simulations, we held the input phase screens constant and varied the number of actuators N_{act} across the entrance pupil to achieve varied Strehl ratios. We both calculate the Strehl ratios from each realization individually, and from an average of all realizations for a given actuator density.

3. STREHL RATIO COMPUTATION TECHNIQUES

While every Strehl ratio measurement technique is different, they share several major common points. If the measurement is being done on image plane data, the diffraction pattern of the telescope is created and then normalized to have the same total intensity as the PSF. The Strehl ratio is then the ratio of the peak intensity of the PSF divided by the peak intensity of the diffraction pattern.

The diffraction pattern is often computed analytically using the equation for a centrally obscured circular aperture

$$P(\nu) = \frac{2J_1(\nu) - 2fJ_1(f\nu)}{(1-f^2)^2\nu^2}$$

where f is the fractional obscuration and $\nu = \theta\pi D/\lambda$, with θ the angle off-axis. This equation is monochromatic and ignores any secondary support structure.

The diffraction pattern can also be created numerically by using Fourier optics. A binary mask, representing the pupil, is created. The Fourier transform of this mask is the complex wavefront at the focal plane of the telescope. The modulus squared of the complex amplitude yields the diffraction pattern. The pixelated approximation of the pupil can lead to errors in the diffraction pattern. When there are only a small number of pixels across the pupil, not all pixels will be fully illuminated. If nothing is done, then the diffraction pattern will be misshapen. This is dealt with by assigning partially illuminated pixels a value between zero and unity based upon the area of the pixel intersected by the pupil.

Once the diffraction pattern has been obtained, it must be scaled to the energy in the PSF. This energy is normally computed by totaling all the energy in a region centered on the PSF peak. The region ideally would be circular, but often square regions are used for computational ease. The optimal size of this region is a topic of debate: The region must be large enough to encompass all the energy of the PSF, but not to encompass pixels with pure noise. Any errors in debiasing, dark subtraction, flat fielding, or sky subtraction will bias this measurement.

Finally the peak energy of both the PSF and diffraction pattern needs to be measured. The simplest way to do this is to use the energy value of the peak pixel. This has several drawbacks in that the peak of the PSF is not guaranteed to fall on a single pixel. Even if it does, due to nonzero pixel size the peak energy will be binned with values that are less than the peak energy, hence lowering the measured value. Interpolation is often used to get around this difficulty.

Equation 1 gives the definition of Strehl ratio in terms of the image plane, but it is also possible to do the computation in the Fourier plane,

$$S = \frac{\int OTF_{\mathrm{PSF}}(\mathbf{u})d\mathbf{u}}{\int OTF_{\mathrm{diff}}(\mathbf{u})d\mathbf{u}}, \tag{3}$$

where $OTF_{PSF}(\mathbf{u})$ is the optical transfer function (OTF) of the image, $OTF_{diff}(\mathbf{u})$ is the OTF of the diffraction limited optical system and $\mathbf{u}$ is the frequency domain vector. The definition assumes that the maximum value of the PSF is located at $\mathbf{x} = 0$. If the maximum value of the measured image is not at $\mathbf{x} = 0$, the term inside the integral must be multiplied by a phase factor, $e^{2\pi i \mathbf{u}\mathbf{x}}$, where $\mathbf{x}$ is the location of the maximum of the image. Normally the image is recentered to avoid having to use the phase factor.

The two techniques are mathematically equivalent, but in practice there are a few differences. In the Fourier plane, it is possible to filter the image to eliminate frequencies higher than the diffraction limited cut-off frequency, which are guaranteed to be pure noise.

It is important to note that the OTF is a complex quantity in general even though the PSF is real. Because the PSF is real the OTF must be Hermitian; that is,

$$OTF(-\mathbf{u}) = OTF(\mathbf{u})^*. \tag{4}$$

In this case the integral in Eq. 3 and the Strehl ratio will be real because the complex part of the OTF will integrate to zero. Occasionally Equation 3 has been written with the modulation transfer function (MTF) instead of the OTF. This is most likely done because the MTF is insensitive to pixel offsets of the PSF. In most cases the OTF and its absolute value the MTF are not identical therefore the MTF should not be used to compute the Strehl ratio. The MTF is a positive definite function so the integral of the MTF is always greater or equal to the integral of the OTF, because the integral of the imaginary portion of the OTF (which is Hermitian) integrates to zero in Eq. 3. In experiments on data from real AO systems, the MTF Strehl ratio was higher by as much as 10%.[4]

4. ERRORS IN STREHL MEASUREMENTS

The Strehl ratio measurement problem is closely related to the problem of adaptive optics photometry, a notoriously challenging area.[5,6] We present a brief summary of some of the theory involved, without intending to be comprehensive.

Using the same notation as in Eq. 1, we normalize the diffraction pattern to have the same total intensity as the observed PSF: $P' = P(\Sigma I)/(\Sigma P)$. Then the Strehl ratio is

$$S = \frac{I(\mathbf{x}=0)}{P'(\mathbf{x}=0)} = \frac{I(\mathbf{x}=0)}{\Sigma I}\frac{\Sigma P}{P(\mathbf{x}=0)}.$$

There will be some error ϵ in computing the total flux of the observed PSF: $\Sigma I' = \Sigma I + \epsilon$; this is just the photometric uncertainty. We assume that there is no photometric uncertainty for the perfect PSF. Then

$$S_{measured} = \frac{I(\mathbf{x}=0)}{\Sigma I + \epsilon}\frac{\Sigma P}{P(\mathbf{x}=0)} \approx S(1 - \epsilon/\Sigma I).$$

Thus the fractional error in measured Strehl ratio is essentially equal to the fractional photometric error $\epsilon/\Sigma I$. By estimating the fractional photometric error we can set limits on how well we ought to be able to measure Strehl ratio given a perfect algorithm.

The photon noise contribution to fractional photometric error will be $\sqrt{\Sigma I}/\Sigma I$, with intensity measured in photons. The sky background will also contribute photon noise. If the mean background intensity is B photons/pixel, then the standard deviation will be $\sqrt{B}$ per pixel. This gives a total error $\sqrt{nB}$, where n is the number of pixels used for the photometry.

It is important to note that while the *fractional* error in sky background $\sqrt{nB}/nB$ goes down as n increases, the *absolute* error $\sqrt{nB}$ goes up. This is important because if n becomes too large the fractional sky error will overwhelm the total stellar flux ΣI (which approaches a constant for large n).

Since we do not know the background level of real data, we must estimate it from a sky region surrounding the PSF. If this region contains n_{sky} pixels, each with error $\sqrt{B}$, then our estimate of the mean background will itself be uncertain by $\sqrt{B/n_{sky}}$, and thus our estimate of the total sky count inside our photometry aperture will be uncertain by $n\sqrt{B/n_{sky}}$.

Summing these contributions, we can now write the fractional uncertainty in the photometry as

$$\frac{\epsilon}{\Sigma_n I} = \frac{1}{\Sigma_n I}\left(\frac{1}{\sqrt{\Sigma_n I}} + \sqrt{nB} + n\sqrt{B/n_{sky}}\right)$$

We have added the subscript n to the summation to emphasize that the total intensity depends on the size of the photometry region. Consider the dependence on n: Increasing the size of the photometry region will add more signal as $\Sigma_n I$ includes a larger fraction of the extended PSF halo, but will also add more sky noise. For sufficiently large n, the noise will overwhelm the signal and the Strehl ratio measurement will be degraded. Based on an analysis of the signal to noise of the observed PSF, we should be able to derive an optimal photometry aperture which minimizes the uncertainty of our Strehl estimate.

In reality, nothing is this ideal. Systematic errors in flat fielding or nonuniform sky backgrounds will likely increase the uncertainty in the sky background subtraction beyond what we have estimated here. It seems likely that this will be the dominant source of error in real-world Strehl measurements, and it remains to be seen if we can derive an optimal photometry aperture in the face of such complications.

5. SPECIFIC STREHL RATIO ALGORITHMS

In this section, we describe the individual algorithms used at the start of the measurement campaign. Many of these algorithms evolved over the course of the campaign as areas for improvement became clear.

5.1. Method One

The diffraction pattern is computed from the analytical equation for the diffraction pattern of a centrally obscured circular aperture, at the center of each pixel of the measured PSF and with the central wavelength of the filter used in the data acquisition. The energy in the PSF is computed by measuring the enclosed energy in a circle with variable radius centered on the peak pixel of the PSF. The radius is normally 2.5", based on the examination of co-added AO images from several AO systems. The diffraction pattern is then weighted by this power and the Strehl ratio is computed by dividing the maximum of the PSF by the maximum of the weighted diffraction pattern.

5.2. Method Two

The diffraction pattern is computed from the analytical equation for the diffraction pattern of a centrally obscured circular aperture. Photometry of the PSF and diffraction pattern is performed using a 2" circular aperture, with a surrounding 0.5" annulus used for sky level estimation. The PSF and the diffraction pattern are registered to subpixel resolution by cross-correlation, and then the PSF is shifted to have the same center as the diffraction pattern. The Strehl ratio is computed from the ratio of peak pixel intensities in both images.

5.3. Method Three

A sky background estimate is made from an annulus surrounding the circular aperture. The median of this background is subtracted from each pixel in the image. Photometry of the PSF image is computed using a variable radius circular aperture. The method uses two techniques of measuring the maximum of the image and averages the results. The first technique fits a two-dimensional Gaussian to the PSF and takes the maximum of the Gaussian as the peak. The second method computes the peak pixel using a cubic-convolution interpolator. In either case, the resulting peak value is compared to a lookup table of peaks measured with the same algorithm for rebinned simulated monochromatic data, where the simulated data is generated with a pixelated hard-edged pupil.

5.4. Method Four

This method used the "Strehl" command in the European Southern Observatory Eclipse software package *.

5.5. Method Five

First peak-centered images of the measured data are created by Fourier shifting the PSF images. The peak location is found to the nearest pixel and then for Nyquist sampled data a 3x3 pixel box is used to compute the sub-pixel position of the peak. A 5x5 box is used for oversampled data. The image is then Fourier shifted by adding a tilt-term to the Fourier phases. This process is an iterative process and normally gets the peak to a fifth of a pixel.

A weighted pixelated pupil is generated at a spatial scale comparable to the image scale of the data, in other words the radius of the cut-off frequency of the modulus transfer function is the diameter of the pupil. A PSF is created numerically by computing the power spectrum of this pupil using a fast Fourier transform. This generates an oversampled PSF, typically four times Nyquist sampling, which is binned. If the peak of this diffraction pattern is not on a single pixel, then the same Fourier shifting is done as described above. Photometry is performed on a 256×256 pixel square centered on the peak pixels, and the ratio of the appropriately normalized peaks gives the Strehl ratio.

5.6. Method Six

The diffraction pattern is generated numerically from the pixelated pupil. This is shifted to the same pixel location as the peak of the image using Fourier phases. The Strehl ratio is then computed from the ratio of the two peaks.

5.7. Method Seven

The diffraction-limited image is first computed on a four-times oversampled grid using a Fourier transform. The correct pixel size is obtained by binning the oversampled image. The photometry of both the diffraction limited image and the PSF is calculated in a circular aperture with a radius of one arcsecond. A sky background estimate is made from an annulus surrounding the circular aperture. After sky subtraction, both images are normalized by dividing by the photometry. A box surrounding the central peak of the image, with a length of about $4\lambda/D$, is extracted and this subimage is oversampled by a factor of eight using the Fourier transform. The maximum value of this oversampled data is then recorded. This method is applied to both the measured or simulated image and the diffraction-limited image. The ratio of the two maximum values is the Strehl ratio.

5.8. Method Eight

The photometry and sub-pixel peak position of the PSF are measured using SExtractor †. The diffraction pattern is computed from the analytical equation for the diffraction pattern of a centrally obscured circular aperture, centered on the same sub-pixel location as the peak of the PSF. The diffraction pattern is normalized to have the same total power as the PSF. The peak intensity of both the diffraction pattern and the PSF are measured using cubic spline interpolation. The Strehl ratio is the ratio of these two peaks.

*http://www.eso.org/projects/aot/eclipse/
†http://sextractor.sourceforge net/

Table 1. This table shows the measured Strehl ratios from the first set of simulated PSFs. The first part of the table details the measurements of the Nyquist sampled data and the second half details the twice Nyquist sampled data. The numbers along the top row correspond to the method used to compute the Strehl ratio in that column.

Truth	1	2	3	4	5	6	8	Average	Std. Dev.
	32.0%	34.9%	38.8%	32.1%	37.3%	37.0%	47.6%	37.1%	5.3%
91.2%	80.3%	79.9%	82.2%		81.7%	83.4%	81.9%	81.6%	1.3%
94.1%	64.8%	73.0%	87.6%	65.1%	84.7%	80.9%	85.6%	77.4%	9.7%
96.7%	78.6%	81.5%	88.1%	78.9%	86.5%	86.4%	86.4%	83.8%	4.0%
15.2%	14.0%	16.4%	17.8%	15.5%	14.8%	16.6%	19.8%	16.4%	2.0%
42.6%	39.0%	41.7%	43.0%	41.0%	41.6%	42.8%	46.1%	42.2%	2.2%
53.7%	49.2%	53.4%	55.9%	52.2%	52.2%	55.2%	57.7%	53.7%	2.8%
64.9%	59.3%	63.5%	66.1%	62.3%	63.2%	65.8%	66.9%	63.9%	2.7%

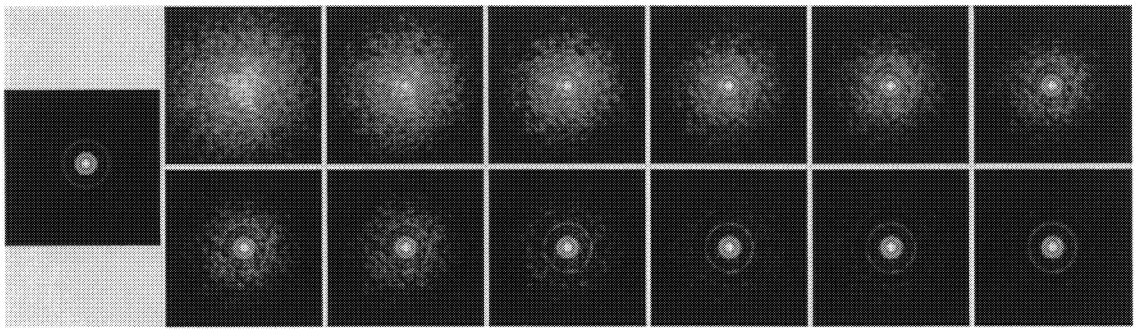

Figure 1. These are the 13 Nyquist sampled PSFs generated in the second data set, shown in a logarithmic scale. The leftmost image is the diffraction limited image. Strehl ratio increase from left to right and from top to bottom for the other 12 images. Each sub-image is 64 pixels across which at a sampling of 45mas/pixel gives a field of view of 2.9". The log scale clearly shows PSF power out to large radii, especially for poorer compensation.

6. RESULTS

The first set of artificial PSFs was generated using the technique in described in subsection 2.1. There were a total of eight PSFs; half were Nyquist sampled and half were twice Nyquist sampled. The true Strehl ratios and the various measured Strehl ratios are shown in Table 1.

This data set confirmed our expectation that different methods produced highly varying estimates of the Strehl ratio, and this was on noiseless data sets. Undoubtedly, it is more difficult to measure Strehl ratios accurately on real data. This data set led to one significant observation: every method underestimated the Strehl ratios for the Nyquist sampled data. However, the simulated data was biased, with most of the Nyquist sampled PSFs having Strehl ratios above 90%, higher than for any of the oversampled data. Was the underestimation due to the Nyquist sampling or the high value of the Strehl ratio?

In the second set of PSFs, we focused on determining what was the major cause of this underestimation. Using the technique described in Subsection 2.2, we generated 24 PSFs which had Strehl ratios ranging from 10% to 90%. Using the same wavefronts, both Nyquist-sampled and twice-Nyquist-sampled PSFs were created. The Nyquist-sampled PSFs are shown in Fig. 1. In addition, we generated a perfect PSF with the same software by setting the wavefront error to zero. This has a Strehl ratio of 1.0 and provides a useful test of each measurement algorithm. The truth and measured Strehl ratios of each of the PSFs are listed in Table 2.

For oversampled data, the standard deviation is less than 1%, which is quite acceptable for most users of Strehl ratio measurements. The standard devation in Strehl ratio from different techniques is much larger for Nyquist

Table 2. This table shows the measured Strehl ratios from the second set of simulated PSFs. The first half of the table details the measurements of the Nyquist-sampled data and the second half details the twice Nyquist-sampled data. The numbers along the top row correspond to the method used to compute the Strehl ratio in that column.

Truth	1	2a	2b	3	4	5	6	7	8	Average	Std. Dev.
11.3%	10.0%	08.7%	11.5%	9.1%	9.7%	9.6%	8.8%	9.9%	11.9%	9.9%	1.1%
19.7%	17.4%	15.7%	20.2%	18.6%	17.0%	18.5%	16.3%	18.7%	19.9%	18.0%	1.6%
28.7%	25.3%	23.3%	29.5%	28.6%	24.7%	28.1%	24.5%	28.1%	28.0%	26.7%	2.2%
37.4%	33.0%	30.6%	38.5%	38.1%	32.2%	37.2%	32.4%	37.1%	35.5%	35.0%	3.0%
44.9%	39.6%	36.7%	46.2%	46.1%	38.6%	44.8%	39.1%	44.7%	42.0%	42.0%	3.6%
56.6%	50.0%	46.3%	58.1%	58.4%	52.6%	56.5%	49.5%	56.4%	52.0%	52.9%	4.5%
61.2%	54.0%	50.1%	62.8%	63.1%	56.0%	61.0%	53.5%	61.0%	55.9%	57.1%	4.9%
65.1%	57.5%	53.3%	66.8%	67.2%	63.4%	64.9%	57.0%	64.9%	59.4%	60.8%	5.2%
73.8%	65.1%	60.3%	75.6%	76.2%	68.3%	73.6%	64.6%	73.6%	67.0%	68.8%	5.9%
79.5%	70.1%	65.0%	81.4%	82.2%	70.7%	79.3%	69.6%	79.3%	72.1%	74.2%	6.4%
82.3%	72.6%	67.3%	84.3%	85.1%	74.2%	82.2%	72.1%	82.2%	74.6%	76.8%	6.7%
86.4%	76.2%	70.6%	88.4%	89.4%	84.5%	86.3%	75.7%	86.3%	78.4%	80.6%	7.0%
100.0%	87.7%	79.9%	100.0%	101.3%		100.0%	87.6%		90.3%	91.4%	8.1%

9.8%	10.1%	9.7%	10.1%	9.1%	10.1%	9.8%	9.6%	9.7%	10.1%	09.8%	0.35
18.6%	19.2%	18.5%	19.2%	18.5%	19.1%	18.8%	18.4%	18.5%	19.3%	18.8%	0.36
28.0%	28.8%	28.0%	29.0%	28.5%	28.6%	28.3%	27.9%	28.0%	28.9%	28.4%	0.41
37.0%	38.0%	37.0%	38.3%	38.1%	37.8%	37.5%	37.0%	37.1%	37.9%	37.6%	0.50
44.6%	45.8%	44.6%	46.1%	46.0%	45.9%	45.2%	44.6%	44.7%	45.4%	45.4%	0.63
56.4%	57.9%	56.3%	58.2%	58.3%	57.8%	57.1%	56.4%	56.4%	57.1%	57.3%	0.80
61.0%	62.6%	60.8%	62.9%	63.0%	62.5%	61.7%	61.0%	60.9%	61.6%	61.9%	0.87
64.9%	66.6%	64.7%	66.9%	67.1%	66.5%	65.7%	64.9%	64.8%	65.7%	65.9%	0.92
73.6%	75.6%	73.3%	75.8%	76.1%	75.0%	74.5%	73.6%	73.5%	74.3%	74.6%	1.03
79.4%	81.5%	79.0%	81.7%	82.1%	81.3%	80.3%	79.4%	79.3%	79.8%	80.5%	1.15
82.2%	84.4%	81.9%	84.6%	85.0%	83.6%	83.2%	82.2%	82.2%	82.8%	83.3%	1.15
86.3%	88.5%	85.9%	88.8%	89.3%	87.8%	87.4%	86.4%	86.3%	87.0%	87.5%	1.18
100.0%	102.0%	96.7%	100.0%	100.7%	98.7%	100.0%	100.0%		97.5%	99.4%	1.72%

sampled data. Though, standard deviation is not a very useful metric for assessing the accuracy of techniques as a function of Strehl ratio, as larger Strehl ratios always have larger standard deviations. It measures the precision of the methods, but not their accuracy.

Fractional Error is a more useful metric for comparing the accuracy of methods. Figure 2 shows the fractional error for the measurements of the second set of PSFs. Fractional error is defined as the measured Strehl ratio divided by the true Strehl ratio. The error curves for each technique are fairly smooth and it may be possible to generate a correction factor for each technique. This would allow comparison between the Strehl ratio values measured by various techniques. This would be useful when comparing AO systems. The fractional error for the oversampled data is larger for smaller values of the true Strehl ratio. The curve of the fractional error for all methods is similar for all methods and much smaller than for the Nyquist sampled data.

The results of this second data set are clear: the Strehl ratios were systematically undersampled for the Nyquist-sampled data. Measurements for the oversampled data are both more accurate and showed less scatter between methods. Unfortunately, most real AO data is Nyquist sampled, or worse yet undersampled. Our results indicate that Strehl ratios reported in the literature for Nyquist-sampled data may err by as much as 5-10%. In particular, comparisons of performance between different AO systems, using different Strehl algorithms, should be considered at least that uncertain.

After some consideration, we identified the underestimation for Nyquist sampled data as due to improperly neglecting the effects of detector pixel size. A pixel with finite size integrates the PSF over some area, rather than sampling it at an infinitely precise point, and thus the peak in pixelated data is reduced compared to the value in sampled data. The Strehl ratio algorithms under investigation here tended to neglect this effect, biasing their results downward. Method 7 takes into account the pixel size and method 5 was modified after the first data set to also take this into account. Both methods generate a oversampled PSF which was then binned to Nyquist sampling. Comparison of the sampled PSF to the binned PSF showed a Strehl ratio reduction of approximately 10

To further investigate this, we modified the software for Method 2 to include this effect. Method 2b is identical to Method 2, except that the diffraction pattern was computed on a four-times-Nyquist-sampled ($\lambda/8D$) grid, and then binned down to Nyquist resolution. The modified code produces Strehl ratios with five to ten times less error than the original code. Similar improvements were seen when the other methods were likewise modified. It remains unclear why the modified Method 2 code slightly overestimates Strehl ratios.

Method 1 did bin down the diffraction pattern for the second data set, but still underestimates the Strehl ratio. This method did not use any sort of recentroiding or interpolation to get the true peak of the PSF. This shows the importance of doing something to compensated for the fact that PSF may not fall exactly on the center of a pixel. The fractional error went down after the method was modified to include an cubic spline interpolation.

We also used the second data set to test the Maréchal approximation: Eq. 2. In the simulation process, a wavefront is created for each PSF. We measured the RMS phase error of each wavefront and converted it to a Strehl ratio. We then compared that Strehl ratio to the "truth" Strehl ratio. This is shown in the left half of Table 3. The agreement is very good and much better than what was anticipated. We also worked backwards, and used the "truth" Strehl ratio to compute the RMS phase error. This is shown in the right half of Table 3. This result shows the validity of the Maréchal approximation.

The results presents here are for noiseless data, and the next data set explores measuring the Strehl ratio in data with realistic levels of read and Poisson noise. The simulations and measurements have been completed, but the analysis is not yet complete and will be presented in a future work.

7. DISCUSSION

The project is still ongoing. At this point, we have learned several things which people should take into account.

1) Strehl ratio measurements for Nyquist-sampled data are generally much less accurate than for oversampled data.

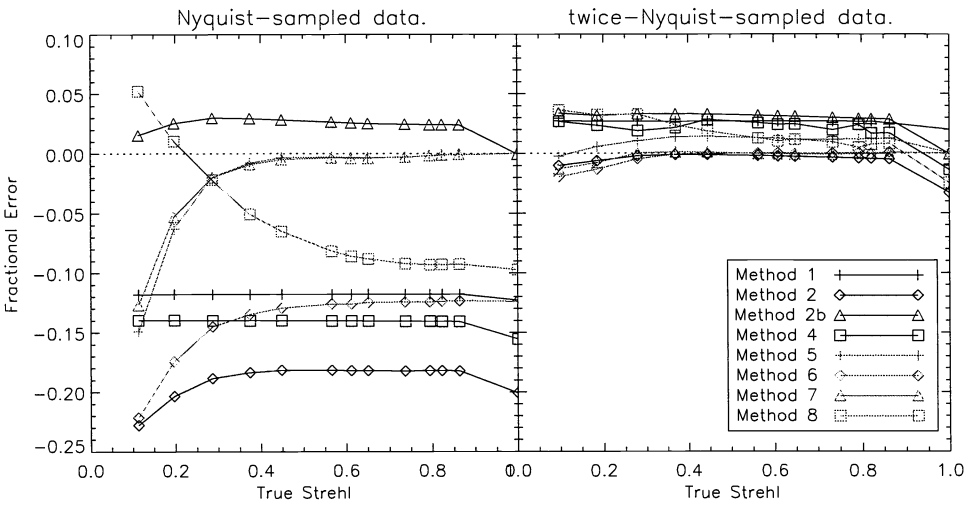

Figure 2. This figure shows the fractional error for the second data set. The left hand side shows the results for the Nyquist sampled data, while the right shows the results for the oversampled data.

Table 3. This table shows the "truth" Strehl ratios, the Strehl ratio computed from the Maréchal approximation, the difference of these two, the RMS phase error computed from the "truth" Strehl ratio, the RMS phase measured from the wavefront used to create the PSF and finally the difference between the two RMS phases.

Truth	Maréchal	Difference	Computed RMS	Measured RMS	Difference
0.113528	0.091450	0.0220776	387.350	409.007	21.6570
0.199824	0.182136	0.0176876	333.242	344.355	11.1131
0.289501	0.278912	0.0105886	292.378	297.758	5.38034
0.375864	0.369834	0.0060308	259.771	262.623	2.85165
0.449140	0.445926	0.0032132	234.943	236.537	1.59303
0.562629	0.562818	-0.0001898	199.154	199.362	0.20801
0.607125	0.607884	-0.0007598	185.508	185.463	-0.04558
0.645984	0.646545	-0.0005610	173.594	173.556	-0.03777
0.732609	0.732805	-0.0001958	146.482	146.473	-0.00934
0.790355	0.790454	-9.858e-05	127.377	127.365	-0.01170
0.818801	0.818854	-5.316e-05	117.416	117.408	-0.00802
0.859876	0.859871	5.781e-06	102.034	102.036	0.00230

2) Comparing Strehl ratios measured by different methods for Nyquist-sampled data should be considered uncertain at the 5-10% level.

3) You should describe your Strehl ratio computation method whenever you report Strehl ratios in a paper. As we have shown, not all Strehl ratios are created equally. Providing information on how the Strehl ratios are computed will allow the reader to put the Strehl ratios in perspective.

4) The computation of the diffraction limited image should take into account the effects of pixel size.

5) The maximum of an image should be measured using some sort of interpolation; otherwise the Strehl ratio will be underestimated.

The project is still ongoing; we are going to continue to refine Strehl ratio algorithms through simulations. Some of the future simulations that we have planned will measure the impact of polychromatic images. Most astronomical data is taken with broadband filters, while the diffraction patterns are usually computed with the central wavelength of the filter.

Another thing we want to investigate is the extent to which neglecting the secondary mirror support spiders affects the measurement of Strehl ratios. Most telescopes have circular apertures with circular obscurations caused by the secondary. The diffraction pattern for this is easily computed. The secondary supports are usually ignored in this computation. It is possible to use a numerical image of the pupil, but it is difficult to get the proper scaling in the image, since the spiders are a very small fraction of the image. This requires a great number of pixels in the numerical image. Segmented mirror telescopes such as the Keck telescopes and Gran Telescopio Canarias have a very similar problem with the segment gaps. It is unclear how to best approach this.

While most AO science cameras are Nyquist sampled, there are a few that are undersampled. These are usually optimized for one wavelength, but sometimes used at a shorter wavelength. Our previous simulations have shown that most algorithms work better with oversampled rather than Nyquist sampled data; it is likely that they perform even worse on undersampled data. We also want to study the effects that subpixel positioning has. We also note that the techniques which use Fourier shifting on either the PSF or diffraction pattern will not be applicable to undersampled data. Thus analytical model fitting of the PSF will be a more suitable technique. However, this will counter the benefits of using the complicated numerical models discussed above.

Our investigation into Strehl ratio has so far shown that there exist appreciable differences and biases between various algorithms for computing Strehl, and that in at least some cases, these biases may be mitigated through simple changes to the software. By determining best practices for Strehl ratio measurement, we hope to minimize systematic errors leading to accurate and unbiased Strehl ratios measured for the wide variety of instruments and conditions encountered in real-world AO imaging. As the project continues, we will make our growing library of sample PSFs available on the Web to maximize participation in this study. We invite all members of the community to test their Strehl ratio codes against our simulations and share the results as we move forward.

ACKNOWLEDGMENTS

This work has been supported by many organizations and we are grateful for that support. They include The National Science Foundation Science and Technology Center for Adaptive Optics, managed by the University of California at Santa Cruz under cooperative agreement No. AST - 987678, and by the Air Force Research Laboratory's Directed Energy Directorate under contract F29601-00-D-0204. M.D.P. is supported by a NASA Michelson Graduate Fellowship. Portions of this work were performed under the auspices of the US Department of Energy by the University of California, Lawrence Livermore National Laboratory, under contract W-7405-Eng-48. Portions of this research were carried out at the Jet Propulsion Laboratory (JPL). JPL is managed by the California Institute of Technology, under contract with the National Aeronautics and Space Administration.

REFERENCES

1. K. Strehl *Z. f. Instrumkde* **22**, p. 213, 1901.
2. J. W. Hardy, *Adaptive optics for astronomical telescopes*, Oxford University Press, New York, 1998.
3. A. Sivaramakrishnan, C. D. Koresko, R. B. Makidon, T. Berkefeld, and M. J. Kuchner, "Ground-based coronagraphy with high-order adaptive optics," *Astrophysical Journal* **552**, pp. 397–408, 2001.

4. L. Roberts, Jr. and C. R. Neyman, "Characterization of the AEOS adaptive optics system," *Pub. Astro. Society of the Pacific* **114**, p. 1260, 2002.
5. O. Esslinger and M. Edmunds, "Photometry with adaptive optics: A first guide to expected performance," *Astronomy and Astrophysics Supplement* **120**, pp. 617–635, 1998.
6. T. ten Brummelaar, B. Mason, H. McAlister, L. Roberts, Jr., N. Turner, W. Hartkopf, and W. Bagnuolo, Jr., "Binary star differential photometry using the adaptive optics system at Mount Wilson Observatory," *Astronomical Journal* **119**, pp. 2403–2414, 2000.